Volume 11, Issue 7, July – 2026 International Journal of Innovative Science and Research Technology
ISSN No:-2456-2165 https://doi.org/10.38124/ijisrt/26jul156

Structural and Electrical Properties of $(Ba_{0.7}Ca_{0.3})TiO_3$-$Ba(Zr_{0.2}Ti_{0.8})O_3$ Ceramics

Ram Kumar[1]; Himanshi Kumari[1]; Sandeep K. Jha[1]; Abhishek Kumar[1]; Kumar P. Chandra[2]; Ajit R. Kulkarni[3]; K. Prasad[1]

[1]University Department of Physics, T.M. Bhagalpur University, Bhagalpur 812007, India
[2]Department of Physics, S. M. College, Bhagalpur 812001, India
[3]Department of Metallurgical Engineering and Materials Science, Indian Institute of Technology, Mumbai 400076, India

Publication Date: 2026/07/22

Abstract: The ceramics exhibiting steady dielectric characteristics across a broad temperature range of operation, particularly exceeding 200°C, present significant potential for the development of high-temperature capacitors. These capacitors are crucial for electronic control systems, especially in hybrid and electric vehicles. One of the extensively researched lead-free perovskite systems $(Ba_{0.7}Ca_{0.3})TiO_3$-$Ba(Zr_{0.2}Ti_{0.8})O_3$ for piezoelectric-based energy harvesting and/or sensing applications. The current study focuses on the pseudo-binary $(1-x)(Ba_{0.7}Ca_{0.3})TiO_3$-$xBa(Zr_{0.2}Ti_{0.8})O_3$; $0 \leq x \leq 1$ ceramic system, synthesized through the standard mixed oxide process. To evaluate the system's performance, X-ray diffraction, dielectric analysis, and AC conductivity studies were performed. The system exhibits high-temperature phase transitions, characterized by a diffusive nature, with transition temperatures varying between 575°C (x = 0) and 620°C (x = 1). The AC conductivity measurements reveal a negative temperature coefficient of resistance, akin to semiconductor-like behaviour, in the prepared ceramic system. This positions the ceramic system as a propitious contender for high-temperature applications.

Keywords: *Ceramic; Lead Free; Solid-State Reaction; Dielectric Constant; Phase Transition; Electrical Conduction.*

How to Cite: Ram Kumar; Himanshi Kumari; Sandeep K. Jha; Abhishek Kumar; Kumar P. Chandra; Ajit R. Kulkarni; K. Prasad (2026) Structural and Electrical Properties of $(Ba_{0.7}Ca_{0.3})TiO_3$-$Ba(Zr_{0.2}Ti_{0.8})O_3$ Ceramics. *International Journal of Innovative Science and Research Technology*, 11(7), 591-595. https://doi.org/10.38124/ijisrt/26jul156

I. INTRODUCTION

Ceramic materials that maintain steady dielectric characteristics at elevated temperatures, particularly in excess of 200°C, are of significant interest for developing capacitors suitable for high-temperature electronic control units in hybrid and electric vehicles. Recently, complex perovskites namely $A(Fe_{1/2}B_{1/2})O_3$; here A represents Ba, Sr, or Ca, and B stands for Nb, Ta, or Sb [1-5]; have received considerable attention due to their impressive dielectric performance ($\varepsilon' \sim 10^3$–10^5) across broad frequency as well as temperature ranges, comparable to the behavior of $CaCu_3Ti_4O_{12}$ [6-10]. More recently, systems such as $Ba_{0.8}Ca_{0.2}TiO_3$–$Bi(Mg_{0.5}Ti_{0.5})O_3$ have demonstrated promising temperature-independent dielectric responses [11,12]. In this context, a relatively newer lead-free ferroelectric system, $(Ba_{0.7}Ca_{0.3})TiO_3$–$Ba(Zr_{0.2}Ti_{0.8})O_3$ (referred to as BCT–xBZT), as proposed by Liu and Ren [13], stands out as a strong alternative to traditional soft $Pb(Zr,Ti)O_3$-based ceramics [14-22]. This system undergoes a relatively low-temperature phase transition near 90°C, posing limitations for high-temperature use. Availability of its dielectric behavior data beyond 200°C, particularly across the full compositional range ($0 \leq x \leq 1$), remains scarce. Previous work of our group has identified an additional phase transition in the high-temperature region for the composition $(Ba_{0.76}Ca_{0.24})(Zr_{0.04}Ti_{0.96})O_3$, backed up by high-temperature *in situ* X-ray diffraction [21]. This work suggests that the BCT–xBZT system may possess complex phase dynamics that are not yet fully understood, particularly at elevated temperatures. The present study, motivated by this gap, explores the dielectric behavior of the $(1-x)(Ba_{0.7}Ca_{0.3})TiO_3$–$xBa(Zr_{0.2}Ti_{0.8})O_3$; $(0 \leq x \leq 1)$ ceramics across the full compositional range with a focus on identifying high-temperature phase transitions. The quality and performance of the present ceramics have been thoroughly assayed by employing X-ray diffraction (XRD), energy-dispersive X-ray spectroscopy (EDS), scanning electron microscopy (SEM), and AC conductivity analysis.

II. EXPERIMENTAL PROCEDURE

Ceramics with the nominal composition $(1-x)(Ba_{0.7}Ca_{0.3})TiO_3$–$xBa(Zr_{0.2}Ti_{0.8})O_3$, where x varies from 0 to 1 in increments of 0.10, were synthesized via the standard mixed-oxide process. The precursor powders were calcined

ISSN No:-2456-2165 https://doi.org/10.38124/ijisrt/26jul156

between the temperatures 1400°C and 1450°C for 5 hours, and were sintered between 1460°C and 1500°C for 4 hours in an air ambiance. The polyvinyl alcohol was used as a binder during the pelletizing process. For carrying out the dielectric measurements, platinum paste was applied to both the flat surfaces of sintered specimens and subsequently heated at 500°C for 30 minutes to ensure good electrode adhesion. Room-temperature powder XRD was performed using CuKα-radiation between the 2θ-range of 10° and 90°. Structural parameters and unit cell details were extracted through Rietveld refinement using the FullProf suite. Surface morphological characteristics of the fractured ceramic specimens were carried out utilizing a field emission type scanning electron microscope (JEOL JSM-7600F, Japan), whereas the dielectric properties were studied using an Alpha high-resolution dielectric analyzer (Novocontrol Technologies) across a broad temperature range (50°C to 800°C) and at 1 kHz as well as 10 kHz.

III. RESULTS AND DISCUSSION

Fig. 1(left) presents the XRD profiles of BCT–*x*BZT ($0 \leq x \leq 1$) ceramics at 30°C. The presence of single-phase sharp peaks without any additional reflections from constituent oxides or carbonates confirms the favorable formation of homogeneous ceramic solid solutions. Also, observed that the XRD peak positions move towards the high Bragg angle side with the addition of BZT to the BCT matrix. The diffraction peaks move toward the higher 2θ side, along with peak splitting, suggesting a reduction in unit cell dimensions or a structural transformation in the crystal lattice as the value of *x* increases. This is because the ionic radii of Ba^{2+} (1.61Å) and Ti^{4+} (0.84Å) are respectively larger than those of Ca^{2+} (0.99Å) and Zr^{2+} (0.74Å), which may be induced due to the generation of strain (lattice distortion) from the mismatching of ionic radius. Therefore, more Ca^{2+} and Zr^{2+} substitution results in a decrease in lattice parameters and hence their volume, which is well supported by the observation that the diffraction peaks shift towards higher Bragg's angle side with increasing *x* (Fig. 1, right). Here, table 1 details the structure of the unit cell along with the lattice parameters as gathered from the XRD analyses.

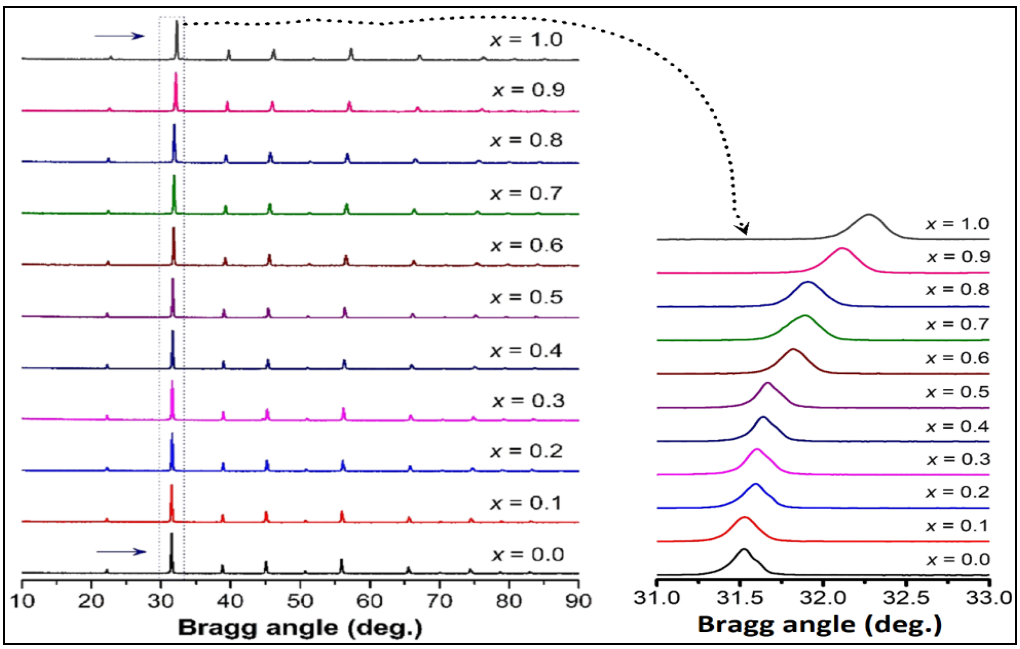

Fig 1 XRD Patterns of BCT–*x*BZT Ceramics at 30°C (left) and XRD Patterns of Selected Region (2θ Range 30.5°–33.0°).

Table 1 Unit Cell Structure and Lattice Parameters of BCT–*x*BZT Ceramics at 30°C

x	System	Space group	Lattice parameter			
			***a* (Å)**	***b* (Å)**	***c* (Å)**	**α = β = γ**
0.0	Cubic	*Pm*3*m*	4.0354(1)	4.0354(1)	4.0354(1)	90°
0.1	Cubic	*Pm*3*m*	4.0270(9)	4.0270(9)	4.0270(9)	90°
0.2	Cubic	*Pm*3*m*	4.0188(3)	4.0188(3)	4.0188(3)	90°
0.3	Tetragonal	*P*4/*mmm*	4.0131(2)	4.0131(2)	4.0106(3)	90°
0.4	Tetragonal	*P*4/*mmm*	4.0063(1)	4.0063(1)	4.0025(4)	90°
0.5	Tetragonal	*P*4/*mmm*	3.9976(6)	3.9976(6)	3.9968(5)	90°
0.6	Tetragonal	*P*4/*mmm*	3.9920(6)	3.9920(6)	3.9913(1)	90°
0.7	Tetragonal	*P*4/*mmm*	3.9931(9)	3.9931(9)	3.9877(2)	90°
0.8	Tetragonal	*P*4/*mmm*	3.9799(7)	3.9799(7)	3.9784(1)	90°
0.9	Tetragonal	*P*4/*mmm*	3.9663(2)	3.9663(2)	2.8047(7)	90°
1.0	Tetragonal	*P*4/*mmm*	3.9563(5)	3.9563(5)	2.7986(9)	90°

ISSN No:-2456-2165 https://doi.org/10.38124/ijisrt/26jul156

It is well established that the dielectric characteristics of various capacitors get affected, even between divergent manufacturers, because of their minor compositional differences. As a result, the room temperature EDS spectra of each ceramic are presented in Fig. 2. The presence of recognized elemental peaks of Ba, Ca, Zr, Ti, and O suggests the pureness of formations of BCT–xBZT ceramics. Also, fractured surface SEM micrographs of the sintered BCT–xBZT ceramics ($0 \leq x \leq 1$) were obtained to assess the microstructural quality, as shown in the insets of Fig. 2. These images reveal a well-developed polycrystalline structure with uniformly distributed grains and minimal porosity, indicating high material density. Grain sizes vary across compositions, ranging between 3–12 μm, and a clear-cut trend of decreasing grain size with increasing x could easily be observed. Such a grain size reduction is likely attributed to stress-induced inhibition of grain boundary mobility during sintering, which restricts grain growth. This suggests a good interaction between the filler particles and the matrix.

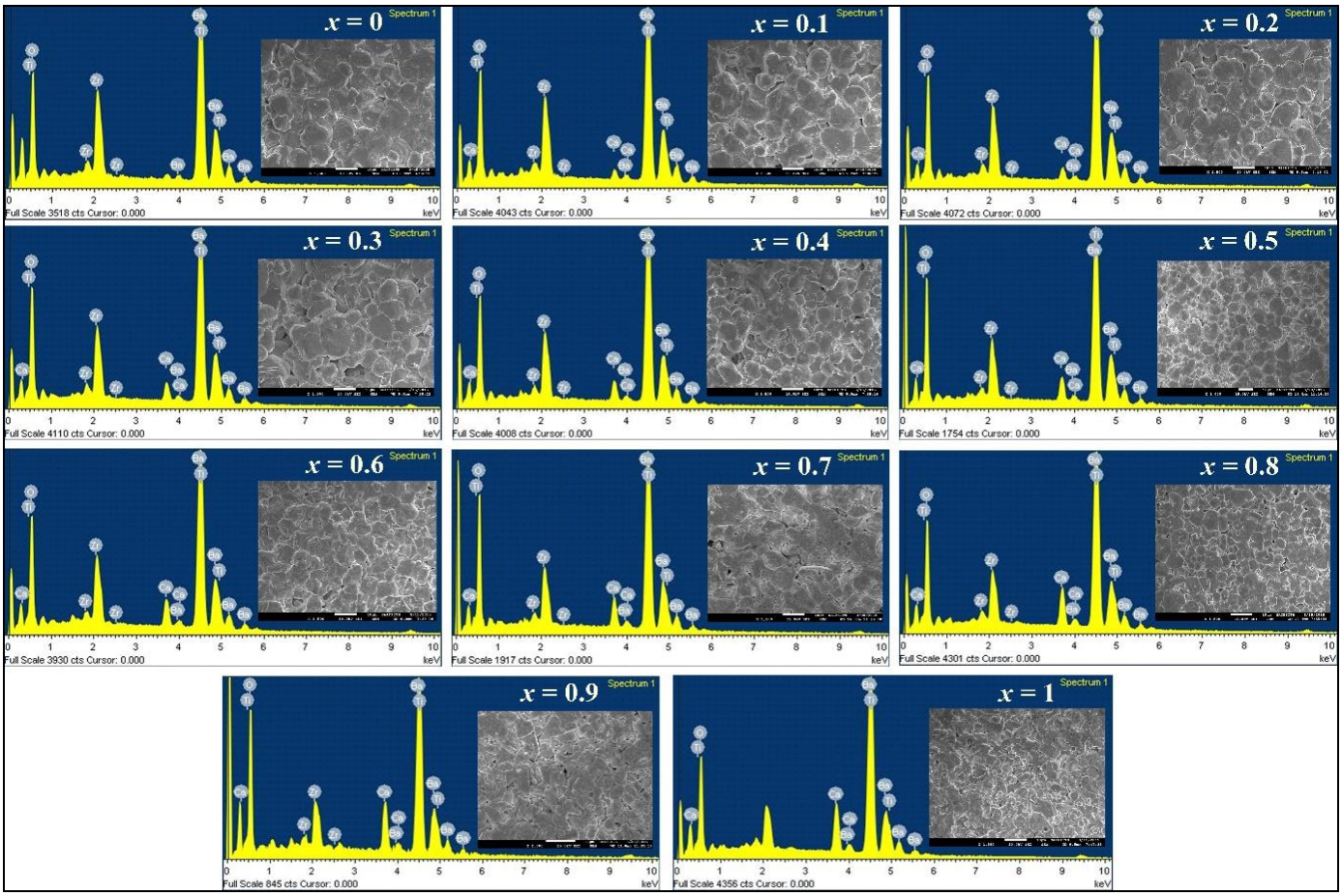

Fig 2 EDS and Scanning Electron Images (Inset) of BCT–*x*BZT Ceramics.

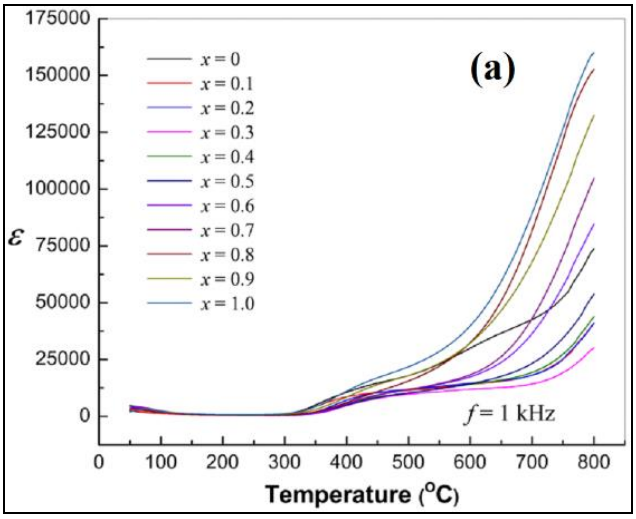

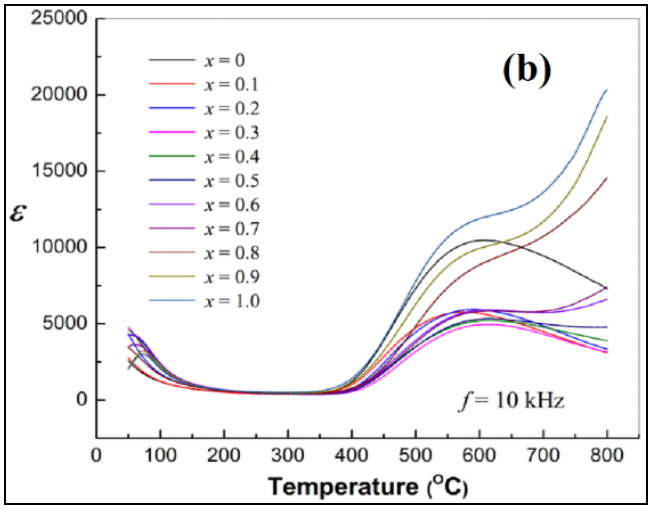

Fig 3 Temperature Dependent Variation of Dielectric Constant at (a) 1 kHz and (b) 10 kHz of BZT–*x*BCT Ceramics.

ISSN No:-2456-2165 https://doi.org/10.38124/ijisrt/26jul156

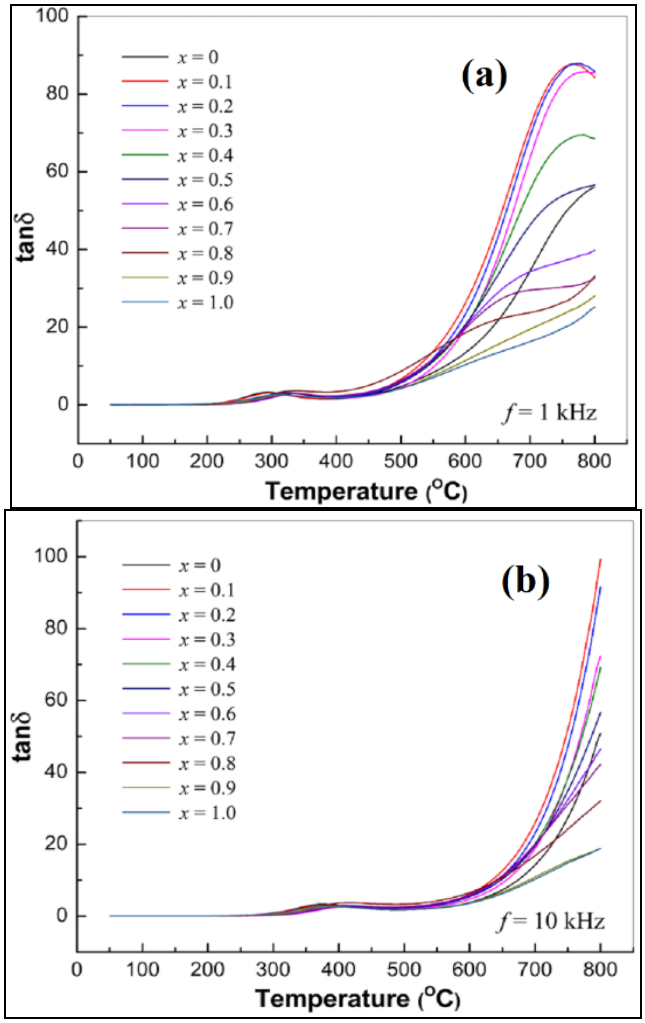

Fig 4 Temperature Dependent Variation of Tangent Loss at (a) 1 kHz and (b) 10 kHz of BZT–*x*BCT Ceramics.

Further, to examine the presence of high-temperature phase transitions present in the BCT–*x*BZT system ($0 \leq x \leq 1$), dielectric measurements were performed across the compositional range. Figs. 3(a) and 3(b) display the temperature-dependent variation of permittivity (ε) at 1 kHz and 10 kHz, respectively. A clear-cut signature of phase transitions at high temperatures is observed, occurring between the temperatures 575°C for $x = 0$ and 620°C for $x = 1$. The observed transitions exhibit a diffuse character, accompanied by notably high values of ε, particularly evident in Figure 3(b). The elevated dielectric response may stem from a combination of intrinsic factors, such as localized changes in electronic structure because of chemical substitutions, and extrinsic influences, including grain boundary effects and grain size variation. A similar behavior could easily be observed for loss tangent (tanδ) *vs.* temperature plots (Figs. 4a and 4b). Besides, the effectively temperature-insensitive region observed between ~180°C to 350°C indicates that the present ceramic system has the potential to be utilized for high-temperature capacitor applications. The room temperature values of ε were observed to be 967, 3284, and 4529, respectively, while that of tanδ was observed to be 0.0078, 0.015, and 0.011 for $x = 0.0$, 0.50, and 1.0 at 1 kHz. Such a low tanδ (~10^{-2}) value is considered beneficial for sensing and energy harvesting applications.

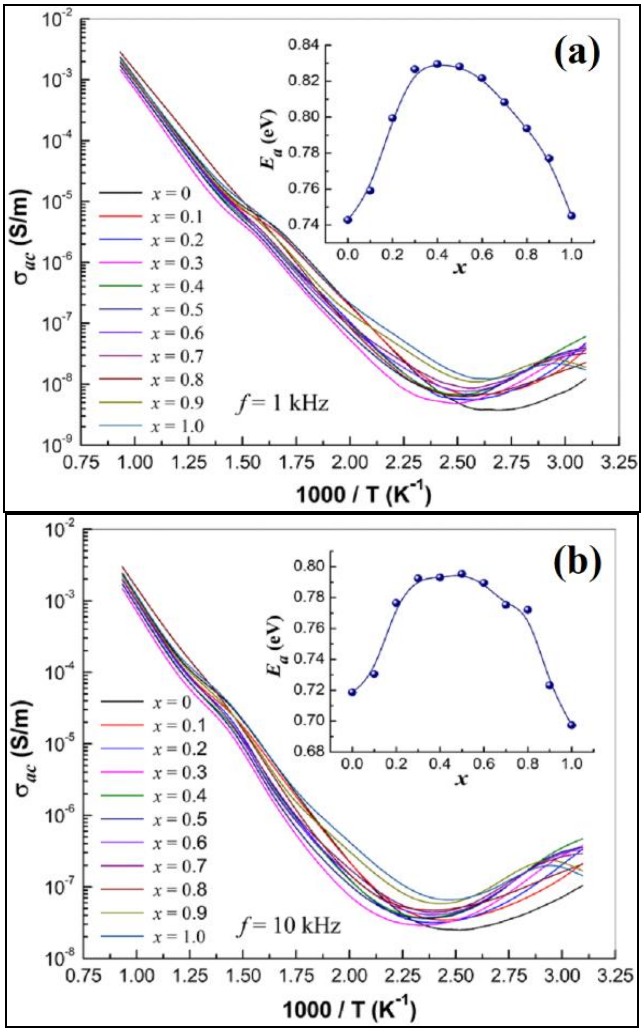

Fig 5 Temperature Dependent Variation of ac Conductivity and Composition Dependence of Apparent Activation Energy (Insets) at (a) 1 and (b) 10 kHz of BZT–*x*BCT Ceramics.

Fig. 5 illustrates the dependence of electrical conductivity ($\log\sigma_{ac}$) on temperature ($10^3/T$) for BZT–*x*BCT ceramics at frequencies of (a) 1 and (b) 10 kHz. In the higher temperature zone, the conductivity behavior pursues Arrhenius relation: $\sigma_{ac} = \sigma_o \exp(-E_a/k_BT)$. By applying a least-squares (linear) fit to the $\log\sigma_{ac}$-$10^3/T$ data, the apparent activation energy ($E_a \approx 0.7$ eV) for conduction was extracted. Also, the values of which increase up to $x = 0.5$ (the MPB composition) and then start decreasing at both frequencies (insets of Fig. 5a and b). An increase in σ_{ac} with rising temperature is also evident, which could be because of the formation of oxygen-vacancies within the bulk material; typically generated during the sintering process, taken up at high temperatures. According to the Kröger–Vink notation: $O_o \rightarrow \frac{1}{2}O_2 \uparrow + V_o^{\bullet\bullet} + 2e^{-1}$, this vacancy formation results in the release of free electrons as a charge compensation mechanism. These electrons contribute to n-type conductivity, exhibiting a negative temperature coefficient of resistance.

ISSN No:-2456-2165 https://doi.org/10.38124/ijisrt/26jul156

IV. CONCLUSIONS

The perovskite-type pseudo-binary ceramic system (1-*x*)($Ba_{0.7}Ca_{0.3}$)TiO_3-*x*Ba($Zr_{0.2}Ti_{0.8}$)O_3 ($0 \leq x \leq 1$, with a compositional step of 0.10) was fabricated via the standard mixed oxide route. X-ray diffraction studies confirmed the single-phase formations of perovskite structure across all compositions. A systematic shift of diffraction peaks toward higher Bragg angles with increasing BZT content (*x*) was observed, attributing a contraction in edge length of the unit cell and/or overall cell volume. Dielectric measurements revealed diffuse-type high-temperature phase transitions occurring within the range of 575°C for $x = 0$ to 620°C for $x = 1$, accompanied by high permittivity values and low tangent loss (~10^{-2}). These features highlight the suitability of this ceramic system for high-temperature capacitor applications, particularly in electronic control units of hybrid and electric vehicles. Furthermore, AC conductivity studies showed negative temperature coefficient of resistance (NTCR) behavior, characteristic of semiconducting materials, reinforcing the potential of the BCT–*x*BZT ceramics for integration into high-temperature electronic devices.

ACKNOWLEDGMENT

Authors are thankful to SAIF, IIT Bombay, Mumbai for providing the XRD data and SEM micrographs.

REFERENCES

[1]. Z. Wang, X.M. Chen, L. Ni, Y.Y. Liu, and X.Q. Liu, "Dielectric relaxations in $Ba(Fe_{1/2}Ta_{1/2})O_3$ giant dielectric constant ceramics," Appl. Phys. Lett., 90, pp. 102905, 2007.

[2]. I.P. Raevski, S.A. Prosandeev, A.S. Bogatin, M.A. Malitskaya, and L. Jastrabik, "High dielectric permittivity in $AFe_{1/2}B_{1/2}O_3$ nonferroelectric perovskite ceramics (A=Ba, Sr, Ca; B = Nb, Ta, Sb)," J. Appl. Phys., 93, pp. 4130, 2003.

[3]. C.-Y. Chung, Y.H. Chang, and G.J. Chen, "Effect of lanthanum doping on the dielectric properties of $Ba(Fe_{0.5}Nb_{0.5})O_3$ ceramic," J. Appl. Phys., 96, pp. 6624, 2004.

[4]. C.C. Homes, T. Vogt, S.M. Shapiro, S. Wakimoto, and A.P. Ramirez, "Optical response of high-dielectric-constant perovskite-related oxide," Science, 293, pp. 673, 2001.

[5]. S. Bhagat, and K. Prasad, "Structural and impedance spectroscopy analysis of $Ba(Fe_{1/2}Nb_{1/2})O_3$ ceramic," Phys. Status Solidi A, 207, pp. 1232, 2010.

[6]. T.-T. Fang, and H.-K. Shiau, "Mechanism for developing the boundary barrier layers of $CaCu_3Ti_4O_{12}$," J. Am. Ceram. Soc., 87, pp. 2072, 2004.

[7]. L. Zhang, "Electrode and grain-boundary effects on the conductivity of $CaCu_3Ti_4O_{12}$," Appl. Phys. Lett., 87, pp. 022907, 2005.

[8]. C.C. Wang, and L.W. Zhang, "Surface-layer effect in $CaCu_3Ti_4O_{12}$," Appl. Phys. Lett., 88, pp. 042906, 2006.

[9]. L. Ni, X.M. Chen, X.Q. Liu, and R.Z. Hou, "Microstructure-dependent giant dielectric response in $CaCu_3Ti_4O_{12}$ ceramics," Solid State Commun., 139, pp. 45, 2006.

[10]. S.M. Ke, H.T. Huang, and H.Q. Fan, "Relaxor behavior in $CaCu_3Ti_4O_{12}$ ceramics," Appl. Phys. Lett., 89, pp. 182904, 2006.

[11]. R. Dittmer, W. Jo, D. Damjanovic, and J. Rödel, "Lead-free high-temperature dielectrics with wide operational range," J. Appl. Phys., 109, pp. 034107, 2011.

[12]. A. Zeb, and S.J. Milne, "Stability of high-temperature dielectric properties for (1-x)$Ba_{0.8}Ca_{0.2}TiO_3$–x$Bi(Mg_{0.5}Ti_{0.5})O_3$ ceramics," J. Am. Ceram. Soc., 96, pp. 2887, 2013.

[13]. W. Liu, and X. Ren, "Large piezoelectric effect in Pb-free ceramics," Phys. Rev. Lett., 103, pp. 257602, 2009.

[14]. H. Bao, C. Zhou, D. Xue, J. Gao, and X. Ren, "A modified lead-free piezoelectric BZT–xBCT system with higher T_C," J. Phys. D: Appl. Phys., 43, pp. 465401, 2010.

[15]. D. Xue, Y. Zhou, H. Bao, C. Zhou, J. Gao, and X. Ren, "Elastic, piezoelectric, and dielectric properties of $Ba(Zr_{0.2}Ti_{0.8})O_3$–$0.5(Ba_{0.7}Ca_{0.3})TiO_3$ Pb-free ceramic at the morphotropic phase boundary," J. Appl. Phys., 109, pp. 054110, 2011.

[16]. V.S. Puli, A. Kumar, D.B. Chrisey, M. Tomozawa, J.F. Scott, and R.S. Katiyar, "Barium zirconate-titanate/barium calcium-titanate ceramics via sol–gel process: novel high-energy-density capacitors," J. Phys. D: Appl. Phys., 44, pp. 395403, 2011.

[17]. P. Mishra, Sonia, and P. Kumar, "Effect of sintering temperature on dielectric, piezoelectric and ferroelectric properties of BZT–BCT 50/50 ceramics," J. Alloys Comp., 545, pp. 210, 2012.

[18]. M.C. Ehmke, J. Daniels, J. Glaum, M. Hoffman, J.E. Blendell, and K.J. Bowman, "Reduction of the piezoelectric performance in lead-free (1-x)$Ba(Zr_{0.2}Ti_{0.8})O_3$-x$(Ba_{0.7}Ca_{0.3})TiO_3$ piezoceramics under uniaxial compressive stress,, J. Appl. Phys., 112, pp. 114108, 2012.

[19]. V.S. Puli, D.K. Pradhan, D.B. Chrisey, M. Tomozawa, G.L. Sharma, J.F. Scott, and R.S. Katiyar, "Structure, dielectric, ferroelectric, and energy density properties of (1-x)BZT–xBCT ceramic capacitors for energy storage applications," J. Mater. Sci., 48, pp. 2151, 2013.

[20]. M. Acosta, N. Khakpash, T. Someya, N. Novak, W. Jo, H. Nagata, G.A. Rossetti, Jr., and J. Rödel, "Origin of the large piezoelectric activity in (1-x)$Ba(Zr_{0.2}Ti_{0.8})O_3$–x$(Ba_{0.7}Ca_{0.3})TiO_3$ ceramics," Phys. Rev. B, 91, pp. 104108, 2015.

[21]. K.P. Chandra, R. Singh, A.R. Kulkarni, and K. Prasad, "High temperature phase transition in $(Ba_{0.76}Ca_{0.24})(Zr_{0.04}Ti_{0.96})O_3$ ceramic," Ferroelectr., vol. 502, pp. 231-239, 2016.

[22]. K.P. Chandra, J.N. Singh, A.R. Kulkarni, R.N.P. Choudhary, and K. Prasad, "Electrical response of $Ba_{0.7}Ca_{0.3}TiO_3$-$BaZr_{0.2}Ti_{0.8}O_3$ solid solution," Mater. Sci. Forum, vol. 1073, pp. 3-9, 2022.